Available online at www.sciencedirect.com
ScienceDirect
Journal of Colloid and Interface Science 314 (2007) 415–421
JOURNAL OF Colloid and Interface Science
www.elsevier.com/locate/jcis

# Positive curvature effects and interparticle capillary condensation during nitrogen adsorption in particulate porous materials

Cedric J. Gommes [a,*], Peter Ravikovitch [b], Alexander Neimark [c]

[a] *Department of Chemical Engineering, University of Liège, Allée du 6 Août 3, B-4000 Liège, Belgium*
[b] *Center for Modeling and Characterization of Nanoporous Materials, TRI/Princeton, Princeton, NJ 08542-0625, USA*
[c] *Department of Chemical and Biochemical Engineering, Rutgers, The State University of New Jersey, Piscataway, NJ 08854-8058, USA*

Received 26 March 2007; accepted 28 May 2007

Available online 2 June 2007

**Abstract**

The adsorption of nitrogen in a collection of spheres that touch or merge in a sintering-like manner is modeled using a Derjaguin–Broeckhof–de Boer approach. The proposed model accounts for both positive curvature effects and for capillary condensation at the contact between two spheres. A methodology is proposed to fit the $P/P_0 > 0.4$ adsorption region with the coordination number of the spheres as the only adjustable parameter. The use of the model is illustrated on a series of silica aerogels. The suitability of various standard isotherms needed for the modeling is also discussed.


*Keywords:* Nitrogen adsorption; Particulate solids; Capillary condensation

## 1. Introduction

An important issue in the characterization of porous materials is the determination of their pore size distribution (e.g., [1,2]). This is typically the purpose of the data reduction software commonly provided with vapor adsorption commercial devices, as for instance methods based on BJH [3] or Broekhoff–de Boer [4] models for adsorption in mesopores. In the frame of these models, the pores are assumed to have a given simple shape. The microstructure of some highly porous solids, however, can be more easily described in terms of the size and shape of their solid skeleton rather than of their pore space. Among others, this is the case of some aerogels with pores of a very complex shape, but with a solid skeleton that can be thought of as a network of simple columns or as aggregates of spheroidal particles.

The physical phenomena that govern the adsorption in these latter solids need not be the same as in most porous solids. It has notably been shown that the convexity of the adsorbent surface in fumed silicas as well as in silica xerogels reduces the amount of nitrogen adsorbed below that adsorbed on a flat surface [5,6]. In some cases the positive curvature of the surface in aerogels can even prevent the occurrence of capillary condensation [7].

The present paper investigates the sorption of nitrogen in a collection of contacting and partially overlapping spheres. The developed model is based on a Derjaguin–Broeckhoff–de Boer (D-BdB) approach and slightly generalizes a model previously proposed by Neimark [8] and by Neimark and Rabinovitch [9] for contacting spheres. A methodology is proposed to fit experimental adsorption data with the coordination number of the spheres as only adjustable parameter, which is illustrated on a series of silica aerogels. The accuracy of the modeling is shown to depend on the choice of an appropriate standard isotherm.

## 2. Materials and methods

### 2.1. Experimental

The silica samples were synthesized by a sol–gel process already described elsewhere [10]. Briefly, the gels are prepared from tetraethoxysilane (TEOS), $H_2O$, ethanol and $NH_4OH$ *via* a single-step base-catalyzed hydrolysis and condensation, with

* Corresponding author.
*E-mail address:* cedric.gommes@ulg.ac.be (C.J. Gommes).

0021-9797/$ – see front matter 
doi:10.1016/j.jcis.2007.05.072

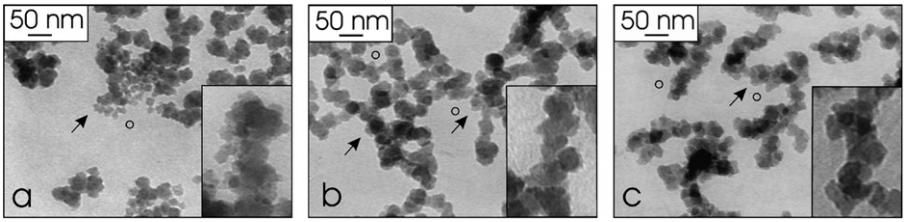


Fig. 1. Example of TEM micrographs of fragments of samples AT025 (a), AT05 (b), and AT40 (c). The circles drawn in the images have a diameter of 15 nm, representative of the particles from which the filaments are made up (arrows). The insets are magnified views of the same samples.

3-aminopropyltriethoxysilane (AES) as co-reactant. The hydrolysis ratio $H = H_2O/(\text{TEOS} + 3/4\ \text{co-reactant})$ is 4 for all gels; the 3/4 factor is justified by the fact that both co-reactants contain three hydrolyzable groups, while TEOS contains four of them. A dilution ratio $R = \text{ethanol}/(\text{TEOS} + \text{co-reactant})$ of 10 is chosen for all samples. Four AES-based samples are analyzed in the present study. The nomenclature is the same as in Ref. [10], the AES samples are labeled AT05, AT15, AT25 and AT40 corresponding to AES/TEOS molar ratios equal to 0.05, 0.15, 0.25 and 0.40, respectively. Aerogels are obtained by drying the gels in supercritical $CO_2$, as described elsewhere [11]. The gels are first aged for seven days at 60 °C, their solvent is afterwards exchanged for acetone, and then for supercritical $CO_2$, followed by a slow isothermal depressurization.

Fig. 1 shows typical transmission electron micrographs of fragments of the aerogels. The images were obtained by crushing the aerogels and by dispersing the powder in ethanol, a drop of which is deposited on a microscopy grid and evaporated. The microstructure of the samples is that of elongated filament-like structures about 50 nm thick, the latter structures being made up of smaller spheroidal particles about 15 nm across. In most cases, the particles are only seen as structures that protrude out of the filaments (arrows in Fig. 1). In the case of sample AT025, however, the particles are sometimes visible individually (Fig. 1a). It should be stressed that the latter preparation did not result in any gel, and it remained liquid; a drop of it was deposited on a microscopy grid and evaporated. The visual inspection of the micrographs suggests that increasing the concentration of AES (from Figs. 1a–1c) the particles are more compacted together within the filamentary structures [10].

Nitrogen adsorption and desorption isotherms are measured at 77 K on a Carlo Erba Sorptomatic 1990 volumetric device, after outgassing the samples overnight at room temperature at a pressure lower than $10^{-4}$ Pa. Fig. 2 shows the adsorption and desorption isotherms measured on the aerogels. Globally the isotherms are typical of non-porous or macroporous samples. Apart from pressures very close to the saturation, there is only a very slight hysteresis. Aerogels are very soft materials that can undergo a significant deformation under the capillary forces that appear during nitrogen sorption. As the latter effects are particularly significant during desorption [12], only the adsorption branch of the isotherms shall be analyzed in the present paper.

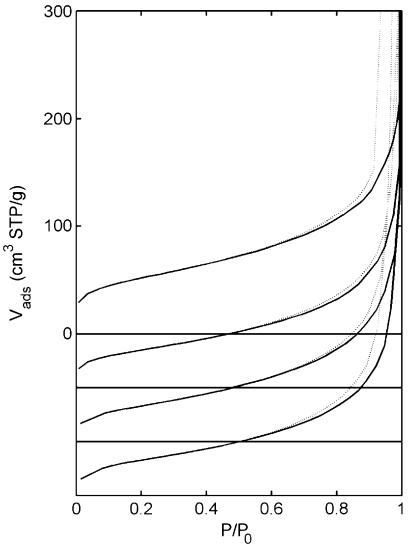


Fig. 2. Nitrogen adsorption (solid line) and desorption (dotted line) isotherms of aerogels AT05, AT15, AT25 and AT40 (from top to bottom). The data were arbitrarily shifted vertically.

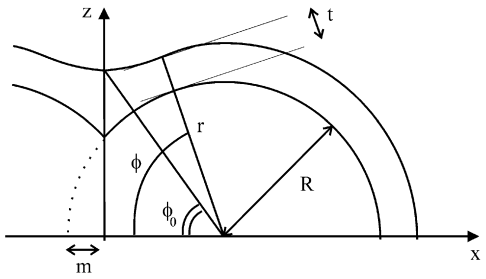


Fig. 3. Coordinates used to analyze the adsorption on two touching spheres and meaning of some symbols. $(r, \phi)$: spherical coordinates, $R$: radius of the spheres, $m$: degree of merging of the spheres, $t$: thickness of the adsorbed film.

### 2.2. Theoretical section

#### 2.2.1. Adsorption on two contacting spheres

The basic element of the modeling is the situation depicted in Fig. 3: two spheres of radius $R$ overlap and merge by a distance $m < R$. Adsorption on such a structure differs from adsorption on a flat surface in two respects. Firstly, since the surface of the sphere has a positive curvature, the thickness of the film adsorbed on it at any given pressure is lower than on a flat surface at the same pressure. Secondly, adsorption is enhanced in the ditch near the contact of the spheres by capillary condensation. These two effects can be accounted for with the D-BdB modeling. The fundamental hypothesis of this approach

is the additive contribution of surface and of capillary forces to the chemical potential of an adsorbate molecule. This leads to the following equilibrium relation for the thickness $t$ of the adsorbed film as a function of relative pressure $P/P_0$ (e.g., [4])

$$\Pi(t) - 2\gamma K(t) = -\frac{R_g T}{V_m} \ln\left(\frac{P}{P_0}\right), \tag{1}$$

where $\Pi(t)$ is the disjoining pressure [13] that depends on the thickness of the polymolecular adsorbed film, $K(t)$ is the average curvature of the free surface of the adsorbate, $\gamma$ is the surface tension of the adsorbate, $R_g$ is perfect gas constant, $T$ is the absolute temperature, and $V_m$ is the molar volume of the adsorbate. In the following, the disjoining pressure shall be replaced by the standard isotherm $F(t)$ defined by

$$F(t) = \frac{V_m}{R_g T}\Pi(t), \tag{2}$$

the name which derives from the fact that, from Eq. (1), the thickness of the film adsorbed on a flat surface with $K = 0$ at pressure $P$ obeys $F(t) = -\ln(P/P_0)$. We also define the length $\lambda$ by $\lambda = \gamma V_m/R_g T$. In order of magnitude, $\lambda$ is the size of the droplet of adsorbate that has the same surface and thermal energies. For nitrogen at 77 K, with $\gamma = 8.85$ mJ/m$^2$ and $V_m = 34.6$ cm$^3$/mol (e.g., [14]), one has $\lambda = 4.78$ Å.

The case of adsorption on an isolated sphere [5] is handled by setting $K = 1/(R+t)$ in Eq. (1), which leads to

$$\frac{2\lambda}{R+t} = F(t) + \ln\left(\frac{P}{P_0}\right). \tag{3}$$

Solving Eq. (3) enables to estimate the thickness $t_R(P/P_0)$ of the film adsorbed on a sphere of radius $R$. As both sides of Eq. (3) are positive and the left-hand side is a decreasing function of $R$, it can be seen that $t_R(P/P_0)$ for any finite value of $R$ is lower than the thickness of the film adsorbed on a flat surface.

To analyze the adsorption on two merging spheres, the average curvature $K$ is expressed in cylindrical coordinates. Assuming an axial symmetry, Eq. (1) becomes [8]

$$\lambda\left[\frac{1}{z(1+\mathrm{d}z/\mathrm{d}x)^{1/2}} - \frac{\mathrm{d}^2z/\mathrm{d}x^2}{(1+(\mathrm{d}z/\mathrm{d}x)^2)^{3/2}}\right] = F\big(t(z,x)\big) + \ln\left(\frac{P}{P_0}\right), \tag{4}$$

where $z(x)$ is the position of the free surface of the adsorbate (see Fig. 3). The boundary conditions that have to be used to solve Eq. (4) are:

$$\left.\frac{\mathrm{d}z}{\mathrm{d}x}\right|_{x=0} = 0, \tag{5}$$

$$z|_{x=2R-m+t} = 0 \tag{6}$$

and

$$\left.\frac{\mathrm{d}z}{\mathrm{d}x}\right|_{x=2R-m+t} = -\infty, \tag{7}$$

where it has to be noted that the thickness $t$ at $x = 0$ and at $x = 2R - m + t$ are unknown quantities that have to be determined by solving Eq. (4).

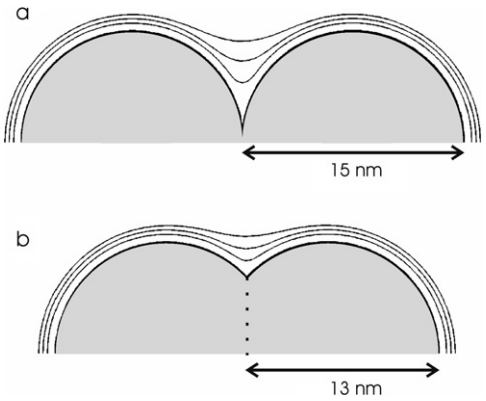


Fig. 4. Example of two touching spheres of diameter 15 nm, and the calculated free surface of the adsorbed film at $P/P_0 = 0.4$, 0.8 and 0.95, from Eq. (8). In (a) the sphere are simply in contact, and in (b) the spheres overlap by $m = 2$ nm. The standard isotherm used for the calculation is FHH2.

Using spherical coordinates $(r, \phi)$ (see Fig. 3), Eq. (4) can be written as [9]

$$\lambda\left[\frac{-r\ddot{r} + 2\dot{r}^2 + r^2}{(\dot{r}^2+r^2)^{3/2}} + \frac{r - \dot{r}ctg(\phi)}{r(\dot{r}^2+r^2)^{1/2}}\right] = F(r-R) + \ln\left(\frac{P}{P_0}\right), \tag{8}$$

where the notations $\dot{r} = \mathrm{d}r/\mathrm{d}\phi$ and $\ddot{r} = \mathrm{d}^2r/\mathrm{d}\phi^2$ have been used. The boundary conditions in Eqs. (5)–(7) become

$$r(\phi_0) = (R-m)/\cos(\phi_0), \tag{9}$$

$$\dot{r}(\phi_0) = -(R-m)/\sin(\phi_0), \tag{10}$$

$$\dot{r}(\pi) = 0. \tag{11}$$

Equations (8)–(10) are identical to Eqs. (2)–(5) of Ref. [9] for $m = 0$, i.e., when the spheres touch without overlapping.

If the standard isotherm $F(t)$ is known, the system of Eqs. (8)–(10) can be solved for any given value of $P/P_0$, $R$ and $m$. The numerical procedure is as follows [9]. The new dependent variable $p = \dot{r}/r$ is introduced in order to transform Eq. (8) into a system of two coupled first-order equations for $r$ and $p$. That system can afterwards be solved by a Runge–Kutta numerical method [15]. Note that $\phi_0$ is an unknown quantity in Eqs. (9) and (10). The value of $\phi_0$ is therefore chosen iteratively in such a way that solving Eq. (8), with Eqs. (9) and (10) as initial conditions, provides a solution $r(\phi)$ that satisfies Eq. (11) with a given accuracy.

Anticipating the discussion of Section 2.3.1 about the choice of an appropriate function $F(t)$, Eqs. (8)–(11) were solved for spheres of diameter 15 nm. Fig. 4 illustrates the shape of the free surface of the adsorbed nitrogen film for touching spheres ($m = 0$ nm, Fig. 4a) and for interpenetrating spheres ($m = 2$ nm, Fig. 4b). For $P/P_0$ lower than about 0.4 the free surface of the adsorbate has the same shape as the surface of the spheres; only at larger relative pressures does the ditch between the two spheres fill by capillary condensation.

### 2.2.2. *Adsorption on a collection of contacting spheres*

The results obtained for adsorption on two contacting spheres can be generalized to a collection of contacting sphe-

res—with more than one point of contact per sphere—by assuming that the contribution of each contact point to the adsorption is additive.

The contribution of a single sphere to the volume adsorbed at the point of contact of two spheres is calculated as follows. The volume of the axisymmetrical envelope defined by $r(\phi)$ is calculated as [9]

$$V = \pi \int_{\phi_0}^{\pi} r^3 \sin^2(\phi)\big(\sin(\phi) - p\cos(\phi)\big)\,\mathrm{d}\phi. \tag{12}$$

The volume adsorbed, $V_{\mathrm{ads}}(P/P_0; R, m)$, is obtained by subtracting from Eq. (12) the volume of the truncated sphere

$$V_{\mathrm{sphere}} = \frac{4}{3}\pi R^3 - \pi m^2 R\left(1 - \frac{1}{3}\frac{m}{R}\right), \tag{13}$$

where the first term in the right-hand side is the volume of a full sphere, and the second term is the volume of the spherical cap that is lost due to its overlapping with the neighboring sphere (see Fig. 3). In the following, we shall define $\Delta V(P/P_0; R, m)$ as the extra volume adsorbed at the points of contacts, compared to an isolated sphere of radius $R$, i.e.,

$$\Delta V = V_{\mathrm{ads}} - \frac{4}{3}\pi\big[(R + t_R)^3 - R^3\big], \tag{14}$$

where $t_R$ is the solution of Eq. (3). Note that $\Delta V$ can be positive if the capillary condensation at the contact point is the leading adsorption phenomenon; it can also be negative because of the surface loss that results from the overlapping of the spheres.

In a collection of contacting and overlapping spheres, if the coordination number $N_C$ (equal to the number contact points per sphere) is low enough, the adsorbed volume per sphere can be written as

$$V_{\mathrm{ads}} = \frac{4}{3}\pi\big[(R + t_R)^3 - R^3\big] + N_C \Delta V. \tag{15}$$

To analyze the role of the different adsorption phenomena, it is instructive to normalize the latter volume by the geometrical surface of the solid, such that it is expressed as an average thickness of the adsorbed film. This leads to

$$t_{\mathrm{avg}} = \left[\frac{4}{3}\pi\big[(R + t_R)^3 - R^3\big] + N_C \Delta V\right] \Big/ \big[4\pi R^2 - N_C 2\pi m R\big], \tag{16}$$

where the denominator is the surface of a sphere from which $N_C$ spherical caps of height $m$ have been removed.

Equations (15) and (16) assume that each contact point contributes in an additive way to the volume adsorbed. This assumption can only be justified if $N_C$ is not too large. Realistic values of $N_C$ are above $N_C = 2$, which is the minimum value that guarantees the connectivity of the spheres, and below $N_C = 12$, which is the largest possible value corresponding to a hexagonal or a face-centered-cubic packing. When a significant merging of the spheres occurs, the largest possible value of $N_C$ is lower than 12. A rough estimation of the maximum permissible value of $N_C$ is

$$N_C < \frac{2R}{m}, \tag{17}$$

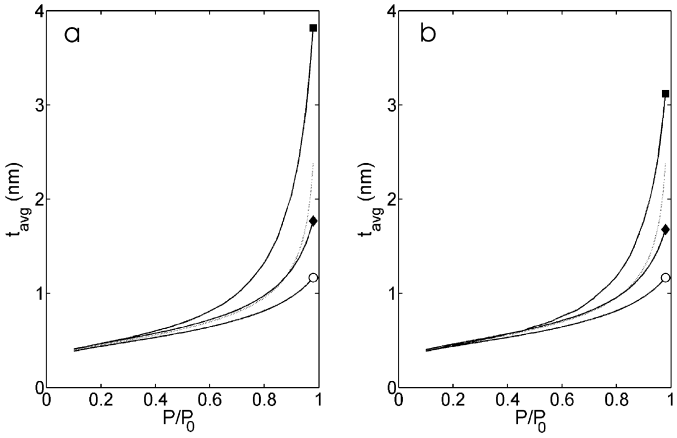


Fig. 5. Predicted amount of nitrogen adsorbed on a collection of touching spheres (a), and on a collection of merging spheres with $m = 2$ nm (b). The data are normalized by the geometrical free surface of the spheres, so that it is an average thickness of the adsorbed film. The dotted line is the standard isotherm used for the calculations (FHH2); (○) is an isolated sphere ($N_C = 0$); (◆) is for $N_C = 2$; (■) for $N_C = 12$ in (a) and $N_C = 5$ in (b).

that is obtained by stating that the surface of the $N_C$ spherical caps, each having a surface $2\pi Rm$, should be smaller than the surface of the sphere, $4\pi R^2$.

Fig. 5 plots the average thickness $t_{\mathrm{avg}}$ obtained from Eq. (16) with $R = 7.5$ nm, $m = 0$ nm (Fig. 5a) and $m = 2$ nm (Fig. 5b). For comparison purposes, the thickness of the film adsorbed on the flat surface is also plotted in Fig. 5, as well as the thickness of the film adsorbed on an isolated sphere of same size, $t_R$, estimated from Eq. (3). All calculated thicknesses almost coincide for $P/P_0 < 0.4$, which means that at low pressure, the adsorption is proportional to the geometrical surface of the adsorbent and it is not dependent on the geometry. Close to the saturation, however, the effects of positive curvature and of capillary condensation can be quite important as they can affect $t_{\mathrm{avg}}$ by a factor 2.

### 2.3. Practical data reduction

#### 2.3.1. Standard isotherms

To analyze experimental adsorption isotherms with the sphere model, the standard isotherm $F(t)$ must be known, as it enters Eq. (8). This is equivalent to knowing the amount of nitrogen adsorbed on a flat surface that is chemically equivalent to the system under investigation. Many such isotherms are reported in the literature for silica, some of which are compared in Fig. 6. FHH1 and FHH2 are two isotherms published under the form of a Frenkel–Halsey–Hill equation [14], $F(t) = Kt^{-m}$ where $K$ and $m$ are constants; $m = 2.241$ for FHH1 [9], and $m = 2.63$ for FHH2 [6,7,16]. The LiC isotherm was measured on a LiChrospher Li-1000 sample [17]. The other three isotherms were published by Hakuman and Naono [18], by Lecloux [2], and by Gregg and Sing [14].

The isotherms displayed in Fig. 6 are expressed as the thickness $t$ of the film adsorbed on the surface. For that purpose, the published adsorption data were first fitted with the BET model in the pressure range from $P/P_0 = 0.05$ to 0.35, in order to estimate the capacity of the monomolecular film (or monolayer)

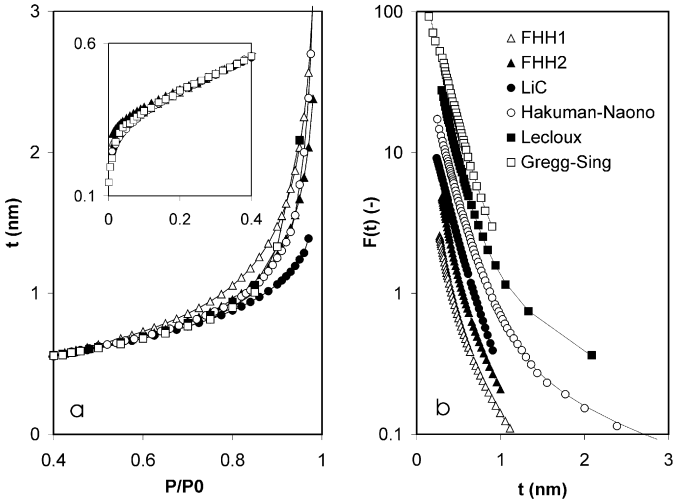


Fig. 6. Comparison of some standard isotherms reported in the literature for nitrogen adsorption on silica, in (a) under the form $t(P/P_0)$ and in (b) under the equivalent form $\ln(P/P_0) = F(t)$: FHH1 [9], FHH2 [6,7,16], LiC [17], Hakuman–Naono [18], Lecloux [2], Gregg–Sing [14]. The inset in (a) is the low pressure part of the standard isotherms; in (b) the curves are shifted vertically; the solid lines are the fits of $F(t)$ with Eq. (18) together with the parameters given in Table 1.

Table 1
Numerical values of the parameters used to fit the standard isotherms with Eq. (18), for $t$ in nanometers

| | $K$ | $m$ | $F_0$ | $\lambda$ (nm) |
|---|---|---|---|---|
| FHH1 [9] | 0.2514 | 2.241 | 0 | –[a] |
| FHH2 [6,7,16] | 0.1971 | 2.63 | 0 | –[a] |
| LiC [17] | 0.0342 | 2.62 | 9.97 | 0.216 |
| Hakuman–Naono [18] | 0.1190 | 1.50 | 12.52 | 0.188 |
| Lecloux [2] | 0.1613 | 1.577 | 19.04 | 0.154 |
| Gregg–Sing [14] | 0.088 | 0 | 15.81 | 0.1886 |

[a] Not applicable.

that covers the surface [1,2,14]. The thickness $t$ was afterwards estimated by dividing the adsorption data by the BET monolayer capacity and by multiplying it by 3.54 Å, corresponding to the generally accepted thickness of a nitrogen monomolecular layer [14].

At low pressure ($P/P_0 < 0.05$) the isotherms in Fig. 6a differ slightly. This has, however, no relevance for the present study that focuses on adsorption phenomena that occur at high relative pressures (see, e.g., the differences between the adsorption curves in Fig. 5). At intermediate pressure, all isotherms in Fig. 6a coincide. This results from the normalization of the isotherms obtained by fitting them with the BET model in the range $0.05 < P/P_0 < 0.35$. At relative pressures larger than $P/P_0 = 0.4$, there is a scatter in the reported standard isotherms, the largest thickness of the adsorbed film corresponding to FHH1 and the lowest to LiC.

For the purpose of easing the numerical calculations, the standard isotherms were fitted with the following equation

$$F(t) = Kt^{-m} + F_0 \exp(-t/\lambda), \tag{18}$$

the numerical values of the parameters are reported in Table 1. It should be noted that the values of parameter $K$ that are reported in Table 1 for FHH1 and FHH2 differ slightly from those in references [9] and [6,7,15] because of the fitting of the isotherm with the BET model, as described above.

### 2.3.2. Fitting procedure

When a given standard isotherm is given, the fitting of the experimental adsorption isotherms with the merging spheres model is done in two steps. First, the experimental isotherms are fitted between $P/P_0 = 0.1$ and $P/P_0 = 0.4$ with the following linear model, often used for $t$-plots analyses [2,14]

$$V(P/P_0) = V_\mu + 0.6478St(P/P_0), \tag{19}$$

where $S$ is the area of the surface on which unhindered polymolecular adsorption occurs and $V_\mu$ is the volume of the micropores. The numerical factor in Eq. (19) is valid for $V$ in $\mathrm{cm}^3$ STP/g, $S$ in $\mathrm{m}^2/\mathrm{g}$ and $t$ in nm. If a sphere model is relevant, $S$ is the geometrical surface area of the spheres and $V_\mu$ is the volume of the micropores that might be present within the spheres. The fitting of the data with Eq. (19) is justified within the sphere model because the model predicts that the average thickness $t_{\mathrm{avg}}$ below $P/P_0 = 0.4$ is the same on a flat surface and on touching spheres (see, e.g., Figs. 4 and 5).

As a second step of the fitting procedure, the values of $S$ and $V_\mu$ are used in Eq. (19) to express the experimental adsorption isotherm as an average film thickness over the entire pressure range. The values of the average thickness are then fitted with Eq. (16) for $0.4 < P/P_0 < 0.98$, by imposing that the geometrical free surface of the sphere is equal to the value of $S$ obtained by the first fitting step. The specific surface is obtained from the surface to volume ratio of a sphere of radius $R$ from which $N_C$ spherical caps of height $m$ are removed; this leads to

$$S = \left[\frac{1000}{2.2}\right]\frac{3}{R}\frac{1-(N_C/2)(m/R)}{1-(3N_C/4)(m/R)^2(1-(m/R)/3)}, \tag{20}$$

where the numerical factor between square brackets is valid for silica with a bulk density of 2.2 $\mathrm{g/cm}^3$, with $R$ in nm, and $S$ in $\mathrm{m}^2/\mathrm{g}$. In the particular case where the radius of the spheres is known from electron microscopy, the constraint of Eq. (20) reduces the number of degrees of freedom to one. The experimental adsorption isotherm can therefore be fitted with a single adjustable parameter, e.g. the coordination number of the spheres $N_C$.

## 3. Results and discussion

Fig. 7 compares the average thickness of the film adsorbed on the aerogels (i) with the thickness of the film adsorbed on a flat surface, and (ii) with the best fit of Eq. (16), for three different standard isotherms, FHH1, LiC and FHH2 (see Fig. 6a). These particular three standard isotherms were chosen because they predict the largest (FHH1), the smallest (LiC), and an intermediate (FHH2) film thickness. The least-square fitting of the isotherms was done by imposing $R = 7.5$ nm, in agreement with the TEM observation (Fig. 1) and with previous characterization work conducted on AES/TEOS xerogels [10]. Therefore, as explained in Section 2.3.2, the only adjustable parameter

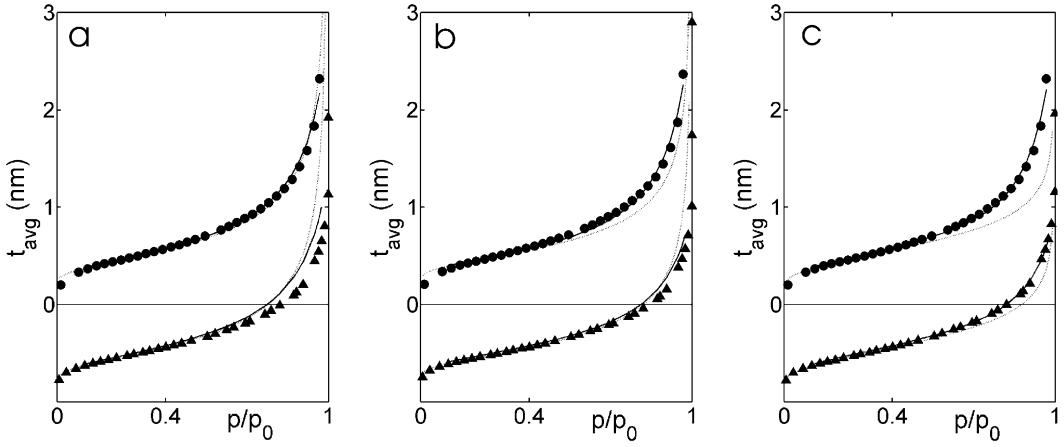


Fig. 7. Experimental average thickness of the film adsorbed on aerogels AT05 (●) and AT40 (▲) determined as explained in the text, using standard isotherms FHH1 (a), FHH2 (b) and LiC (c). The symbols are the experimental values, the dotted line is the standard isotherm, and the solid line is the best fit of the data with Eq. (17) with only the coordination number as adjustable parameter. On each graph, the two samples were arbitrarily shifted vertically.

Table 2
Numerical values of the parameters fitted on the adsorption isotherms of aerogels AT05 to AT40

| | $S$ ($m^2$/g) | | | $V_m$ ($cm^3$ STP/g) | | | $N_C$ (–) | | | $m$ (nm) | | | Error (%) | | |
|---|---|---|---|---|---|---|---|---|---|---|---|---|---|---|---|
| AT05 | 178 | 164 | 161 | 5 | 0 | 6 | 2.0 | 2.0 | 4.2 | 0.8 | 0.3 | 0.44 | 7 | 4 | 1 |
| AT15 | 124 | 121 | 124 | 0 | 0 | 0 | 2.8 | 3.4 | 5.7 | 2.4 | 1.9 | 0.9 | 4 | 3 | 2 |
| AT25 | 119 | 117 | 119 | 0 | 0 | 0 | 2.8 | 4.2 | 6.9 | 2.7 | 1.5 | 0.8 | 2 | 4 | 3 |
| AT40 | 117 | 114 | 117 | 0 | 0 | 0 | 3.0 | 4.6 | 7.4 | 2.4 | 1.5 | 0.8 | 2 | 3 | 2 |

$S$ and $V_\mu$: specific surface area and microporous volume. $N_C$: coordination number of the spheres. $m$: degree of merging of the spheres. Error: average relative error of the fit. The three numbers in each column correspond to the use of three different standard isotherms: from left to right FHH1, FHH2 and LiC.

left to fit the model for $0.4 < P/P_0 < 0.98$ is $N_C$. For the fitting, the value of $N_C$ was bound to stay larger than 2, which is the minimum possible value to have a connected structure. The numerical values of the fitted parameters are reported in Table 2: $S$ and $V_\mu$ were obtained from the fit of the data at $0.1 < P/P_0 < 0.4$ with Eq. (19), $N_C$ was obtained from the fit at $0.4 < P/P_0 < 0.98$ with Eq. (16), and $m$ is the only possible value compatible with Eq. (20) for the obtained values of $S$ and $N_C$ with $R = 7.5$ nm.

As visible in Fig. 7, all standard isotherms enable to fit properly the adsorption on aerogel AT40. However, the estimated coordination number of the spheres varies significantly as it passes from 3 with FHH1 to more than 7 with LiC, and the estimated degree of merging of the spheres is also quite different (Table 2). Globally, for whichever of the used standard isotherms, the values of the fitted parameters for AT40 are realistic with a coordination number $N_C$ larger than 2 and a degree of merging $m$ that is a fraction of the radius of the spheres.

For aerogel AT05, the sphere model with standard isotherms FHH1 and FHH2 strongly overestimates the actual adsorbed volume, while the use of LiC enables to fit the isotherm properly. There are two possible explanations for the overestimation of the adsorption by the model. The first one would be that the size of the particles was overestimated: at a given pressure, the thickness of the film adsorbed is smaller for smaller particles, in agreement with Eq. (3). This is unlikely to be the reason here, as it is unlikely from TEM that the particles be significantly smaller than 15 nm (Fig. 1). Another possible explanation would be that the microporous volume was underestimated: increasing $V_\mu$ would indeed flatten the adsorption isotherm at high pressure. It has to be noted that the fitting of Eq. (19) is a state-of-the-art way of estimating the microporous volume, e.g., when $t$-plots are done [2,14]. Furthermore, it is clear from the qualitative shape of the isotherms (Fig. 2) that the samples are not significantly microporous. Therefore, a significant error in the estimation of $V_\mu$ is also unlikely.

The question has therefore to be addressed of the suitability of the various published standard isotherms to analyze adsorption phenomena close to the saturation, and of the reliability of the results they yield. When standard isotherms are compared, this is often done in the prospect of analyzing the microporosity of samples and the analysis focuses on low pressures [2,14,17]. The analyses seem to overlook the scatter of the various standard isotherms in the high pressure region, which is the main focus of the present study, and which is also of some practical importance when such methods as BJH [3] or Broekhoff–de Boer [4] are used to determine mesopore size distributions. It is not sufficient that the adsorbents on which standard isotherms are measured be non-porous, their surface has to be strictly flat. The scatter in the values of $t$ in Fig. 6 may have various origins. A surface roughness at the nanometer scale may lead to reversible capillary condensation that would lead to an overestimation of $t$. On the other hand, a positive curvature of the surface may lead to an underestimation of $t$.

The fact that the use of FHH1 and FHH2 leads to an overestimation of the amount adsorbed on aerogel AT05 suggests

that these standard isotherms overestimate the actual thickness of the film adsorbed on a flat silica surface. On the other hand, the use of LiC enables to fit properly all the investigated adsorption isotherms with realistic values of the coordination number of the spheres.

## 4. Conclusions

A model was proposed for analyzing the adsorption of nitrogen at 77 K on a collection of contacting spheres. The model is based on the Derjaguin–Broekhoff–de Boer approach, and it slightly generalizes a model initially proposed by Neimark [8] and by Neimark and Rabinovitch [9] by allowing the neighboring spheres to overlap in a sintering-like manner.

It is shown that the adsorption below $P/P_0 = 0.4$ is almost not affected by the geometry of the adsorbent, but only by its specific surface area. At larger pressure, if the coordination number of the spheres is low the adsorption is dominated by the positive curvature of the spheres, by which the amount adsorbed is lower than on a flat surface of the same area. On the contrary, if the coordination number of the spheres is high, the adsorption is dominated by the capillary condensation at the contact of neighboring spheres, and the amount of nitrogen adsorbed is larger than on a flat surface.

A methodology is proposed that enables experimental isotherms to be fitted in the $P/P_0 > 0.4$ region with the coordination number of the spheres as the only adjustable parameter. With an appropriate choice of the standard isotherm, on which the modeling is based, experimental adsorption isotherms of silica aerogels could be properly fitted. The analysis shows that the various investigated aerogels are characterized by a different coordination number of their constitutive particles.

## Acknowledgments

C.J.G. is a postdoctoral researcher of the Belgian National Fund for Scientific Research (FNRS). The authors are grateful to Dr. Arnaud Rigacci of the Ecole des Mines de Paris for making the supercritical drying of the gels, and to Dr. Silvia Blacher of the University of Liège and Dr. George W. Scherer of Princeton University for fruitful discussion. Part of this work was performed during a stay of C.J.G. in Princeton, supported by the ExxonMobil Benelux Chemical Award 2004, by the Camille Héla Foundation of the University of Liège, and by the Patrimoine de l'Université de Liège. This work was also supported by the National Fund for Scientific Research, Belgium, and by the Région Wallonne 'Direction Générale des Technologies de la Recherche et de l'Énergie.'

## References

[1] K. Kaneko, J. Membrane Sci. 96 (1994) 59.
[2] A.J. Lecloux, in: J.R. Anderson, M. Boudart (Eds.), Catalysis: Science and Technology, vol. 2, Springer-Verlag, Berlin, 1981, pp. 171–230.
[3] E.P. Barret, L.G. Joyner, P.H. Halenda, J. Am. Chem. Soc. 73 (1951) 373.
[4] J.C.P. Broekhoff, J.H. de Boer, J. Catal. 9 (1967) 8.
[5] J.H. de Boer, B.G. Linsen, J.C.P. Boekhoff, Th.J. Osinga, J. Catal. 11 (1968) 46.
[6] C.J. Gommes, S. Blacher, J.-P. Pirard, Langmuir 21 (2005) 1703.
[7] G.W. Scherer, J. Colloid Interface Sci. 202 (1998) 399.
[8] A.V. Neimark, Kolloidn. Zh. 47 (1985) 531.
[9] A.V. Neimark, A.B. Rabinovitch, Kolloidn. Zh. 47 (1985) 1103.
[10] C.J. Gommes, M. Basiura, B. Goderis, J.-P. Pirard, S. Blacher, J. Phys. Chem. B 110 (2006) 7757.
[11] A. Rigacci, M.-A. Einarsrud, E. Nilsen, R. Pirard, F. Ehrburger-Dolle, B. Chevallier, J. Non-Cryst. Solids 350 (2004) 196.
[12] G.W. Scherer, D.M. Smith, S. Stein, J. Non-Cryst. Solids 186 (1995) 309.
[13] P.-G. de Gennes, F. Brochard-Wyart, D. Quéré, Capillarity and Wetting Phenomena: Drops, Bubbles, Pearls, Waves, Springer-Verlag, New York, 2004.
[14] S.J. Gregg, K.S.W. Sing, Adsorption, Surface Area and Porosity, Academic Press, London, 1982.
[15] W.H. Press, S.A. Teukolsky, W. Vetterling, B.P. Flannery, Numerical Recipes in C++: The Art of Scientific Computing, Cambridge Univ. Press, Cambridge, 2002.
[16] A.W. Adamson, A.P. Gast, Physical Chemistry of Surfaces, sixth ed., Wiley–Interscience, 1997.
[17] M. Jaroniec, M. Kruk, J.P. Olivier, Langmuir 15 (1999) 5410.
[18] M. Hakuman, H. Naono, J. Colloid Interface Sci. 241 (2001) 127.